Floe size effects on wave-ice interactions: theoretical background, implementation and applications

Guillaume Boutin, Fabrice Ardhuin[a], Dany Dumont, Caroline Sévigny[b], Fanny Ardhuin[a]

[a] *Univ. Brest, CNRS, IRD, Ifremer, Laboratoire d'Océanographie Physique et Spatiale (LOPS), IUEM, Brest, France*
[b] *Institut des Sciences de la Mer, Université de Québec à Rimouski, Rimouski, Quebec, Canada*

Abstract

A model with a consistent representation of wave energy and dispersion in the presence of variety of sea ice conditions is presented. The ice is treated as a single layer that can be fractured in many floes expected to be equivalent to circular floes with a power law distribution of diameters. This layer of ice induces a dissipation of the wave energy through basal friction and secondary creep associated with ice flexure, in addition to an energy-conserving scattering. Academic cases aiming to reproduce a simplified Marginal Ice Zone (MIZ) are used to discuss the effects of each process separately. Attenuation is exponential for all processes, with strong dependencies on the ice thickness and floe sizes for scattering and creep. Scattering triggers an increase in the wave height at the ice edge due the reflected energy in open water, and significantly broadens the wave directional spectrum for short period waves. The cases are then forced by wave spectra extracted from a 2010 hindcast of a documented ice break-up event in Svalbard, ant it appears that only creep consistently reproduces the observations. Eventually, running the model on a 12.5km resolution Arctic grid emphasizes the need for a mechanism to ensure wave energy dissipation in broken ice, plausibly under-ice friction.

Keywords: sea ice, floes, spectral wave model

1. Introduction

Sea ice is going through a dramatic evolution, both in the Arctic (e.g. Stroeve et al., 2007) and in the Southern Ocean (Nghiem et al., 2016).

Changes in sea ice cover and thickness are not fully understood and probably combine thermodynamic effects with mechanical effects. Among the latter, waves can play an important role in the break-up of the ice cover, which is becoming more important in the Arctic with an increase of wave heights over the last 20 years (Stopa et al., 2016b) that is probably caused by a larger area of open water available for wave growth (Thomson and Rogers, 2014; Asplin et al., 2012). Because wave generation is expected to be negligible in ice-covered regions and waves are strongly attenuated at the ice edge, numerical wave models have often treated pack ice as land, with no wave present (Tolman, 2003). There is, however, a transition region where wave motion is significant, and that we shall call the Marginal Ice Zone (MIZ), with a width that can be as large as a few hundreds of kilometers. Waves are responsible for either limiting the size of ice pancakes during their growth or breaking the ice layer into floes. In return, wave propagation can be strongly modified by the ice and the attenuation of waves propagating from the open ocean is expected to depend strongly on the ice properties (Squire et al., 1995). Here we will ignore the conditions with frazil ice or pancake ice when multiple layers of ice can be found in the water, these are discussed by e.g. de Carolis et al. (2005), Wang and Shen (2010) and Rogers et al. (2016). Instead, we focus on the the interaction of waves with a layer of ice that can deform elastically, and can be broken into floes. The different mechanisms that have been proposed to explain the wave attenuation in the ice can be represented by wave-ice interaction source terms in the wave action equation that describes the evolution of the wave field (Masson and LeBlond, 1989). The importance of these mechanisms is still unknown (Squire, 2007). Wadhams (1973) emphasized the importance of wave dissipation by secondary creep, namely the anelastic dissipation of waves due to the ice flexure. Later work, following the Marginal Ice Zone EXperiment (MIZEX) have rather emphasized the multiple reflection of waves by the floes, and scattering has been generally accepted as a dominant source of wave attenuation (Kohout and Meylan, 2008; Kohout et al., 2014; Montiel et al., 2016). Yet, for measured long period swells in the middle of the Arctic, Ardhuin et al. (2016) showed that the peaked times series of swell energy and the narrow directional spectra were not consistent with a significant scattering, and rather proved that the swell attenuation was due to dissipative processes. They also found that the recorded wave heights were consistent with a creep-induced dissipation using flow law coefficients determined by the laboratory experiments of Cole et al. (1998). Other dissipative processes, such as the friction below a single ice layer as proposed by Liu and Mollo-Christensen (1988) cannot reproduce the attenuation when using a proper transition between laminar and turbulent conditions (Stopa et al., 2016b). However, both the friction under the ice and the creep dissipation are based on an the assumption of a single continuous ice layer. Here we propose a generalization of the parameterization proposed by Wadhams (1973) to random waves and the possible break-up of the ice layer into floes. We combine this creep dissipation with an update of the scattering and ice break-up parameterizations proposed by Dumont et al. (2011) and Williams et al. (2013a), who considered the feedback of the ice break-up by waves on the scattering. Our modification consists of conserving the scattered wave energy by redistributing it from incident to reflected directions. The purpose of this paper is to present a consistent treatment of wave-ice interactions in the presence of ice floes and to discuss the complex wave attenuation patterns that may occur. We thus present in section 2 the four processes that we consider here, namely creep dissipation, under-ice friction, ice break-up and scattering. Numerical simulation in academic but representative situations are presented in section 3, followed by discussions and conclusions in section 4.

2. Physical processes and parameterizations

The evolution of the wave action spectrum $N(k, \theta)$, discretized on a spectral grid with fixed frequencies f and direction θ is given by the Wave Action Equation. The evolution of the spectrum on a spherical Earth with longitude λ and latitude ϕ,

$$\frac{\partial N}{\partial t} + \frac{1}{\cos\phi}\frac{\partial}{\partial\phi}\dot{\phi}N\cos\theta + \frac{\partial}{\partial\lambda}\dot{\lambda}N + \frac{\partial}{\partial k}\dot{k}N + \frac{\partial}{\partial\theta}\dot{\theta}_g N = \frac{S + S_{\text{ice}}}{\sigma}\,, \qquad (1)$$

in which the the processes related to the ice are included in the energy source terms S_{ice}. The various advection velocities in physical (λ, ϕ) and spectral (k, θ) spaces are given by (Tolman and Booij, 1998; The WAVEWATCH III ® Development Group, 2016). The ice effects are further decomposed as scattering, creep and basal friction (Stopa et al., 2016c),

$$S_{\text{ice}} = S_{\text{ice},scat} + S_{\text{ice},creep} + S_{\text{ice},fric}. \qquad (2)$$

Our under-ice friction $S_{\text{ice},fric}$ combines the viscous expression by Liu and Mollo-Christensen (1988) using the kinematic viscosity of sea water at the freezing point, $\nu_w = 1.83 \times 10^{-2}$ cm^2 s^{-1}, and a turbulent part defined by analogy with bottom boundary layers (Grant and Madsen, 1979), with the dissipation rate controlled by the roughness length for the wave motion. This combination is based on transition in terms of Reynolds number, with Rayleigh-distributed wave heights, each wave having a Reynolds number (see Stopa et al., 2016c, for details).

2.1. Wave propagation and energy

Following Wadhams (1973), we consider the ice as a continuous thin elastic plate over the water. Solving for the linearized equations of motions, he found that the water motion is the same as under surface gravity waves without ice, with only a change of dispersion relation from the de Laplace (1776) dispersion relation without ice,

$$\sigma^2 = gk \tanh(kD) \tag{3}$$

where σ is the radian frequency of the wave, k the wavenumber and D is the water depth. This gives a phase speed C and group speed C_g. Now with an ice layer of constant thickness h_i and density ρ_i, less than the water density ρ_w, and an effective Young modulus Y^*, the flexural rigidity of the ice is

$$L = \frac{Y^* h_i^3}{12(1-\nu^2)}, \tag{4}$$

where ν is Poisson's ratio for sea ice set to 0.3. With the ice cover, the dispersion relation (3) becomes

$$\sigma^2 = \frac{\rho_w g k_i + L k_i^5}{\rho_w \coth(k_i D) + \rho_i h_i k_i} \tag{5}$$

where we now use the notation k_i for the wave number in the presence of ice. This gives a group speed,

$$C_{g,i} = \frac{\partial \sigma}{\partial k_i} = \frac{\rho_w g + (5\rho_w + 4\rho_i h_i k_i) L k_i^4 - (3\rho_w + 2\rho_i h_i k_i) k_i^2}{2\sigma(\rho_w + \rho_i h_i k_i)^2} \tag{6}$$

The stiffness of the ice thus makes the short waves relatively faster, similar the the effect of surface tension for capillary waves (Figure 1). We note that alternative dispersion relations are discussed by Mosig et al. (2015). Another important change in the presence of ice is the relation between the surface elevation amplitude a and the density of mechanical energy per unit horizontal surface. Indeed, due to the ice elasticity, a significant part of the energy may be potential elastic energy. Wadhams (1973) defined the ratio R of the total energy per unit surface E_t and the energy of the waves of same amplitude in the absence of ice,

$$R = 1 + \frac{4Y^* h^3 \pi^4}{3\rho g \lambda_{ice}^4 (1 - \nu^2)}. \tag{7}$$

In conditions where wave energy is conserved, an amplitude a propagating from the open ocean becomes a_i in an ice-covered region. Neglecting refraction and reflection we have

$$C_g \frac{a^2}{2} = C_{g,i} R \frac{a_i^2}{2}. \tag{8}$$

Hence, the surface elevation amplitude of short waves propagating from the open ocean to ice-covered water can be strongly reduced. This effect is particularly important when considering the break-up of a continuous layer of ice by waves, as the wave amplitude may jump by a factor $\sqrt{R}$ when the ice breaks. In order to avoid numerical errors associated to such jumps when the ice is reformed or broken, or at boundaries between model forced by inconsistent ice parameters, we have thus chosen to work, in the model, with a wave action spectrum that is multiplied by $RC_{g,i}/C_g$, and convert the spectrum on output to a measurable surface elevation spectrum, multiplying it by $C_g/RC_{g,i}$.

2.2. Wave scattering by ice floes

Here we follow the general approach of Meylan and Masson (2006), but we use a simplified scattering source term

$$\frac{S_{\mathrm{is}}(k,\theta)}{\sigma} = \int_0^{2\pi} \beta_{\mathrm{is,MIZ}} [s_{\mathrm{scat}} N(k,\theta') - N(k,\theta)] d\theta'. \tag{9}$$

The simplification is that the scattering coefficient β_{is} is taken independent of incident and reflected directions θ and θ', instead of directional distributions given by detailed modelling studies, (e.g. Masson and LeBlond, 1989; Montiel et al., 2016). The parameter s_{scat} is normally equal to 1, but other models have preferred to use $s_{\mathrm{scat}} = 0$ (e.g. Williams et al., 2013a). The scattering coefficients $\beta_{\mathrm{is,MIZ}}$ are estimated following Williams et al. (2013a). Namely the wave reflections are treated as a succession of reflections at straight interfaces between open water and ice, with waves propagating perpendicular to the ice edge. The number of reflections is a function of the ice concentration, and the mean floe diameter $\langle D\rangle$. This value $\langle D\rangle$ is determined by assuming a power law distribution of the floe diameters, a minimum value $D_{\min}$ and a maximum value $D_{\max}$ that is related to the break-up of ice by the waves,

$$\langle D\rangle = \frac{\gamma}{\gamma-1}\left(\frac{D_{\max}^{-\gamma+1}-D_{\min}^{-\gamma+1}}{D_{\max}^{-\gamma}-D_{\min}^{-\gamma}}\right) \tag{10}$$

Here we use $\gamma = 2+\log(F/2)$ with $F = 0.9$, where F is the fragility as defined in Dumont et al. (2011). Previous waves-in-ice model (e.g. Williams et al., 2013a; Dumont et al., 2011) fixed $D_{min} = 20$ m, as it is the limit at which waves with $T_p = 6$ s can bend the floes. Indeed, floes that are much shorter than the wave wavelength generally tilt and do not bend. Assuming that this bending is responsible for most of the scattering (Meylan and Squire, 1996), we chose to define $D_{min} = C_\lambda \lambda_i$ with $C_\lambda \simeq 0.3$, which is coherent with the onset of scattering for waves of period $T_p = 6$ s, in 20 m circular ice floes that are 50 cm thick (Kohout, 2008).

2.3. Ice break-up

The value of $D_{\max}$ is determined from the local sea state, after searching for the shortest waves with wavelength λ_i that are able to break up the ice, giving $D_{\max} = \lambda_i/2$ if and only if the three following criteria are met,

- $\lambda_i/2 \geq D_{\min}$
- $\lambda_i/2 > D_c$, where D_c is the critical diameter, which depends on ice properties, below which no flexural failure is possible
- $\varepsilon(\lambda_i) > \varepsilon_c$, the maximum strain due to the incoming wave has to be greater than a defined critical strain

For the first criterion, ideally we would also impose that $D_{\max}$ can only be reduced over time, but this is only possible when using a coupled wave-ice model in which the value of $D_{\max}$ would be advected and allowed to increase by freezing. The second criterion relies on Mellor (1986), which defines D_c as the minimum diameter for which flexural failure is possible. D_c is equal to

$$D_c = \left(\frac{\pi^4 Y^* h^3}{48\rho g(1-\nu^2)}\right)^{1/4} \tag{11}$$

For the third criterion, which corresponds to the flexural strain threshold, we take the critical strain to be $\sigma_c/[Y^*(1-\nu^2)]$, where σ_c is the ice flexural strength. F_{break} is the ratio of the maximum value of the strain to its root mean square value. In general, this ratio is a weakly increasing function of the duration considered. Here we estimated $F_{break} = 3.6$ by considering the expected maximum amplitude in the succession of $N \simeq 500$ waves with Rayleigh-distributed amplitudes, during the time over which the sea state is approximately constant. The horizontal strain caused by waves is related to the curvature of the ice layer, which, in one dimension and for monochromatic waves is

$$\varepsilon = \frac{h}{2}\frac{\partial^2 a_i}{\partial x^2}. \tag{12}$$

Compared to Williams et al. (2013a), taking care of the elastic energy introduce a very important correction in the local amplitude a_i of the sea surface elevation. The other difference is that we define a scale-by-scale strain by partial integration of the spectrum over a given wavelength, similar to the scale-by-scale steepness used by Banner et al. (2000) and Filipot and Ardhuin (2012). We recall that our wave spectrum is formulated in energy and not surface elevation variance, so that the surface elevation variance is reduced by a factor $C_g/RC_{g,i}$, which gives

$$\varepsilon^2(\lambda_i) = \frac{1}{F_{\text{break}}}\left(\frac{h_i}{2}\right)^2 \frac{C_g}{RC_{g,i}} \int_{0.7k_i}^{1.3k_i} k_i^4 F(k) dk \tag{13}$$

where h_i is the ice thickness and $k_i = 2\pi/\lambda_i$.

The update of $D_{\max}$ is a two-steps process. First, the shortest wavelength $\lambda_{i,min}$ for which the condition $\varepsilon(\lambda_i) > \varepsilon_c$ is fulfilled is computed. Then, to account for the possibility of having a narrow spectrum, the selected wavelength ($\lambda_{i,break}$) is the one for which the associated wavenumber $k_{i,break}$ respects:

$$F(k_{i,break})k_{i,break}^4 > F(k_j)k_j^4, \quad \forall j \in \mathbb{N} \mid 0.7k_{i,min} < k_j < 1.3k_{i,min} \tag{14}$$

In summary, our implementation of wave break-up extends the work of Williams et al. (2013a) by

- properly including the effect of elastic energy on the reduction of wave elevation amplitude in unbroken ice. As shown in Figure 3, this can lead to a factor 10 difference for maximum wave heights for ice breaking.

- taking into account the random distribution of wave heights we use the expected maximum local strain, instead of the frequently exceeded root mean square.

In practice these changes are very important. Although the second modification can be absorbed into empirical calibration factors, the first correction considerably reduces the unphysical break-up that would otherwise happen due to even very low level of energy in the high frequency part of the spectrum (Figure 3). Indeed, the version 5.16 of WAVEWATCH III uses a wind input that is scaled by the ice concentration, so that even with 98% ice concentration in the middle of the Arctic, there is still a little energy that could lead to a spurious break-up of the ice. Physically, taking into account the energy flux conservation makes short waves unable to deform thick ice, as most of their energy goes into the elastic deformation of the ice.

2.4. Creep

Wadhams (1973) was the first to propose that creep-induced dissipation, namely the anelastic deformation of ice, could explain the observed attenuation of waves in the pack ice. Here we extend his analysis for monochromatic waves, to the case of random waves. Wadhams (1973) assumed that the relation between strain and stress proposed by Nye (1953) for glaciers could also apply to the oscillating ice motion, with

$$\left(\frac{d\varepsilon}{dt}\right)_{ij} = \frac{\tau^2}{B^3}\sigma'_{i,j} \tag{15}$$

where B is the flow law constant and is a function of ice temperature. This was confirmed by the laboratory experiments of Cole et al. (1998) who estimated the dependence of B on ice temperature. Using a uniform ice temperature near the freezing point of sea water ($270K$) gives a value of $B = 10^7$ N m^{-2}s$^{1/3}$. With details given in Appendix A, this gives a temporal decay coefficient for the wave energy that is

$$\beta_{\text{creep}} = \frac{3}{160} B h_i^5 \left(\frac{Y^*}{2B(1-\nu^2)}\right)^4 k_i^4 \frac{C_g^2}{\rho g C_{g,i} R^2} F \int_{0.7k_i}^{1.3k_i} k_i^4 E(k) dk \tag{16}$$

with F an empirical factor that varies with $D_{\max}$ and λ_i so that if the ice is broken into floes shorter than the wave wavelength, they do not bend, hence creep dissipation should be negligible for such floes. We expect a relatively smooth transition of the dissipation, when averaged over many floes, from a zero dissipation for $\lambda_i \gg D_{\max}$ to the full dissipation rate given by $F = 1$, we have thus chosen a form

$$F = \tanh\left(\frac{D_{\max} - C_\lambda \lambda_i}{0.2 D_{\max}}\right), \tag{17}$$

where $C_\lambda \simeq 0.3$ (same tuning as for D_{min} in 2.3) is an adjustable parameter, and the width of the transition was arbitrarily set to 0.2 $D_{\max}$. Eq. (16) gives the dissipation rate,

$$\frac{S_{\mathrm{creep}}}{\sigma} = -\beta_{\mathrm{creep}} N. \tag{18}$$

2.5. Numerical implementation

Our implementation of wave dissipation and scattering effects in the WAVEWATCH III model (The WAVEWATCH III ® Development Group, 2016) corresponds to the addition of dissipation and scattering term, in the wave action equation. Another important change introduced in the model is a splitting of the ice source terms from the more usual source terms of wind-wave generation, 4-wave nonlinear evolution and wave breaking. With this splitting, the ice source terms are integrated with an implicit method that is well suited for quasi-linear terms. Besides, the ice source terms, with the exception of scattering, are all scaled by c, the ice concentration, while the wind input and the dissipation terms are scaled by $(1 - c)$, to account for the fact that the ice cover prevents the momentum to be transferred from the atmosphere to the ocean.

3. Effects of different processes taken separately

To investigate the effects of the attenuation and ice break-up processes, separately and combined, simple academic tests were realized on a grid with 100×40 nodes, with a 2.5 km resolution. Each test starts with waves radiating into the domain at $x = 0$. The left part of the model domain is free of ice over the first 10 km, followed by a linear increase in ice concentration from 0.4 to 1, as x increases from 10 to 70 km. This set-up roughly represents the ice conditions discussed by Collins et al. (2015). The ice thickness was taken constant over all the ice-covered area. Wave conditions at the forcing boundary are constant with a narrow Gaussian frequency spectrum centered around a fixed peak frequency f_p, with a half width of 0.01 Hz. The distribution of wave energy along the left boundary at $x = 0$ is also Gaussian with a half-width of 5 km and a maximum significant wave height of 3 m. The model was ran without wind input, wave breaking or non-linear source terms. Alternatively, the spectrum at the boundary was replaced by off-ice spectra provided by a realistic simulation of the Arctic using WAVEWATCH III (Stopa et al., 2016b) and corresponding to the event of May 2 and 3, 2010, described by Collins et al. (2015). For that case, we rotated the forcing spectrum so that the direction with the largest density of wave energy is lined up with our x-axis. Figures 4 and 5 illustrate the effects of different processes on ice break up and the associated attenuation of wave heights. Scattering alone does not dissipate energy, and energy grows in time with multiple scattering in the model domain, so that for $T_p \geq 10$ s waves are able to break the ice over the entire length of the domain after a few weeks. We did not wait an equilibrium solution and stopped the simulation after 65h, which is already much longer than a typical storm or swell event, usually limited to 12 h. Waves undergo a noticeable attenuation in the ice covered sea, which perceptibly increases with the ice thickness and the ice frequency. The reflected waves in the open sea prior to the ice edge lead to an increase of the wave height up to $\simeq 2$ m for $T_p = 5$ s . In order to obtain a more realistic behavior, we added dissipation by combining scattering with the weakest possible dissipation effect due to viscous friction below ice plates. Scattering dominates, and if the attenuation is visibly increased, the trends do not suffer any consequent changes. H_s evolution was fit to an exponential law of the form $H_s = H_{s,0}\ e^{-\alpha x}$. Results are summarized in Table 1. As expected, the effective attenuation along the x-axis is exponential, with determination coefficients $R^2 > 0.95$ as long as there is no steep change in $D_{\max}$. When the ice is broken, attenuation rates for waves with ($T_p = 10$ s) are found to be of the same order than the ones reported in Kohout et al. (2014) for $H_s < 3$ m in the Antarctic MIZ, when the attenuation is exponential. For $T_p = 5$ s, the order of magnitude of our attenuation rates is increased by a factor 10. When the ice is unbroken, the attenuation rates fall down with the number of reflections. Figure 6 illustrates an other effect of scattering: an increase in the directional spread of waves which are reflected in all directions, resulting in a broadening of the beam of energy in the y direction. This broadening depends on α, and so increases along with ice thickness and decreases with the wave period.

Figures 4 and 5 also display the effect of friction with and without its tur-

Scattering + Visc. friction	$D_{\max} < 100m$		$D_{\max} > 100m$	
	α	R^2	α	R^2
$T_p = 5$ s , $h_i = 25$ cm	0.047	0.99	0.008	0.99
$T_p = 10$ s , $h_i = 25$ cm	0.002	0.99	/	/
$T_p = 5$ s , $h_i = 1$ m	0.072	0.99	0.025	0.95
$T_p = 10$, $h_i = 1$ m	0.008	0.99	0.004	0.99

Table 1: Values of the attenuation rates supposing an exponential attenuation α (km^{-1}), and the associated determination coefficient R^2 for various combination of wave period and ice thickness when scattering and viscous friction are activated.

bulent part. As expected from the parameterizations, the friction-induced attenuation is a little sensitive to the ice thickness due to both the $C_g/RC_{g,i}$ factor and the effect of the dispersion relation on the wavelength, but it strongly increases when the period reduces. This effect is mostly due to the temporal dissipation proportional to $k_i/\sqrt{T_p}$ for the viscous part, giving an attenuation distance proportional to $T_p^{3.5}$. For waves with periods over 10s, the viscous dissipation has very little impact on the scale of the domain considered here, with only a 33% reduction in wave energy over 200 km for $T_p = 10$ s. A transition to turbulent dissipation, for a boundary layer Reynolds number of the order of 10^5, typically increases the dissipation rate by up to a factor 10 when using a roughness length of 1 cm (Stopa et al., 2016a). However, the Reynolds number is affected by the wave height decreases, and for low wave heights the effect of turbulence vanishes (see Table 2).

$T_p = 5$ s $h_i = 25$ cm	$H_s > 1m$		$H_s < 1m$	
	α	R^2	α	R^2
Viscous only	0.011	0.99	0.008	0.013
Visc. + Turb.	0.098	0.98	0.015	0.97

Table 2: Values of the attenuation rates supposing an exponential attenuation α (km^{-1}), and the associated determination coefficient R^2 for friction with and without the turbulent term, with $T_p = 5$ s and $h_i = 25$ cm in the domain.

Creep-induced dissipation gives a very strong attenuation near the ice edge where the wave height is still large, provided that the ice is not broken, an a much lower dissipation rate further into the ice (see Table 3). In practice, creep dissipation is the process showing the greatest dependency on both wave period and ice thickness. Short waves are attenuated to undetectable levels for periods around 5 s, and this attenuation strongly depends on the ice thickness. In particular, we find that thin ice, with $h_i = 0.25$ m produces a stronger attenuation than thicker ice with $h_i = 1$ m. This counter-intuitive result is caused by the $C_g/RC_{g,i}$ which strongly depends on the ice thickness, as shown by Figure 7. Indeed, for short waves propagating into unbroken ice, without any dissipation the wave amplitude is strongly reduced by the factor $\sqrt{C_g/RC_{g,i}}$. For the shortest periods this amplitude reduction more than compensates the increase in dissipation due to an increase in h_i. That compensation is less for longer periods, giving a maximum attenuation as a function of the wave period, as shown in Figure 7. Things get more complex once the ice is broken (Figure 7.b). In that case, wave attenuation critically depends on the wavelength λ_i compared to $D_{\max}/C_\lambda$. The main effect of ice breaking is to reduce the attenuation of the longer periods, as they correspond to the longer wavelengths. In thin ice however, waves wavelengths are weakly increased compared to thick ice cases, so that when break-up occurs, the effects of F are mitigated. Nevertheless, in a general way, dissipation strongly decreases for long period waves, to the point it almost vanishes for $T_p = 15$ s and $h_i = 0.25$ m.

Creep $T_p = 10$ s , $h_i = 1$ m	α	R^2
$D_{\max} < 120m$	0.078	0.58
$120m < D_{\max} < 200m$	0.003	0.97
$D_{\max} > 200m$	0.001	0.99

Table 3: Values of the attenuation rates supposing an exponential attenuation α (km^{-1}), and the associated determination coefficient R^2 for $T_p = 10$ s and $h_i = 25$ cm when only creep is activated.

4. Model evaluation

In the previous section we have shown that, unless other dissipation mechanisms are scaled by ad hoc factors (e.g. Liu et al., 1991), creep produces the strongest attenuation. Creep is also very sensitive to ice break. For broken ice, the attenuation is dominated by under-ice friction for wave periods over 5 s, except in the case of very thick floes or if the wave height is too low to trigger turbulence. We now evaluate the effect of all processes and their combinations in several realistic conditions.

4.1. Svalbard swell event of May 2, 2010

Here we reproduce the conditions observed to the south of Svalbard on May 2 and 3, 2010, as described by Collins et al. (2015). Figure 8 show the effects of the activation of each process on the wave attenuation and the floe size distribution with the Svalbard conditions at the western boundary. Under the effects of scattering and friction, H_s decreases progressively as waves propagate further into the ice. Except in the case of the full friction term with thin ice floes ($h_i = 25$ cm), the domain ends entirely broken at the end of the simulation. Creep acts differently from the other processes discussed above. For very thin ice ($h_i = 25\ cm$), short waves are strongly damped at the ice edge, which results in a substantial loss of energy. It prevents the ice from being broken in small floes, and as a consequence does not lead to a break-up event similar to Collins et al. (2015) description. Nevertheless, in this latter paper, floes are reported to be $50 - 60$ cm thick. In this case (Figure 8.b & 8.e), the domain can be divided into two parts:

- The western part, with broken ice, weak attenuation and high H_s.
- The eastern part, with unbroken ice, and low H_s

Between these two parts, waves create a front characterized by strong gradients of $D_{\max}$ and H_s, which becomes narrower as the ice thickness increases (Figures 8.c & 8.f). Note that for the floe size diameter, it exists a second front which corresponds to an initial fracture by long waves ($\lambda_i \simeq 300m$). The activation of all the processes results in H_s and $D_{\max}$ distributions dominated by the creep dissipation, but the add of each process damps the shortest waves enough to prevent from the ice being broken. As a consequence, we observe a very strong attenuation at the ice edge, not agreeing what Collins et al. (2015) suggests. Unfortunately, in the absence of trustful data concerning the ice thickness, the ice concentration and the floe sizes from the ice edge to the boat position, it is hard to assess the quality of this test case quantitatively speaking.

Collins et al. (2015) observations also offer the opportunity to discuss our tuning of C_λ. Figure 9 shows both the H_s profile spatially after 12 hours of run duration and its temporal evolution at a given point of the domain – roughly representing the distance at which the boat was from the ice edge. $C_\lambda = 0.5$ leads to a smooth and relatively slow transition from 50 cm waves to 3 m ones in about, and was therefore rejected. On the opposite, $C_\lambda \leqslant 0.2$ dissipates too much energy as soon as it encounters sea ice (top panel of Figure 9), while Collins et al. (2015) reported that there was almost no attenuation after the break-up occurred. Finally, having to choose between 0.3 and 0.4, the former was preferred as it shows a steep H_s increase from about 1 m to over 3 m in about 1 hour, against more than 2 hours for $C_\lambda = 0.4$ (bottom panel of Figure 9).

4.2. A realistic model of the Arctic

The model has been eventually ran on a stereographic polar grid of the northern hemisphere (see Stopa et al., 2016b, for details) with the ice concentration and thickness being forced by the Arctic Ocean Physics Reanalysis (1991-2014) provided by CMEMS (`http://marine.copernicus.eu/`) and based on TOPAZ4 reanalysis products (Sakov et al., 2012). The model is forced by the 3-hourly ERA-Interim 10m neutral winds (Dee et al., 2011). The source terms are those of Ardhuin et al. (2010). Initially, $D_{\max}$ is set to $D_{max\ init} = 1000$ m. The period tested was May 2010.
Strong (2012) suggested that the MIZ could be defined as the ice covered area with $0.15 < c < 0.8$, but also as the area of interactions between waves and sea ice Dumont et al. (2011). As the ice concentration and thickness are given by the TOPAZ reanalysis product, the only ice parameter on which waves have an effect is the ice diameter. In such conditions, we chose to define the MIZ as the area where ice has been broken by the waves, *e.g* for which $D_{\max} < D_{max\ init}$, and $c > 0.15$ to ensure a significant presence of ice. In Figure 10, we present the total broken area achieved for each process and some combinations, along with the area achieved with Strong (2012) concentration criterion. The blue line represents the MIZ area when the model is ran with only creep to dissipate the wave energy in the ice. As creep dissipation almost vanishes when the ice is broken, waves tend to penetrate further in the ice, which broadens the MIZ extent in a unrealistic way. As a consequence, creep only cannot explain the wave attenuation in the ice. It has to be associated with friction to avoid breaking the whole Arctic sea-ice after some month of simulations. Note that scattering does not dissipate en-

ergy neither, and consequently a combination of this latter process and creep is not suitable. Just like Williams et al. (2013b), we observe that the concentration criterion and the breaking criterion give different results for the boundary of the MIZ, but with the same order of magnitude. Once again, activating all the processes with their parameters tuned as described in 3 leads to a very reduced MIZ area compared to each process taken separately. To get an idea of what it represents on a map, the MIZ given by all processes and the combination of scattering and viscous friction are reproduced on Figure 10. The snapshot is taken during the storm event on Svalbard, and the MIZ extent in all the Barents sea appears greater than in other regions, such as eastern Greenland. In calm conditions, MIZ extents in these two regions are quite similar. As an order of magnitude, the averaged extent of the MIZ according to the breaking criterion in the region between south-eastern Greenland to north Svalbard in Figure 10 is 37 km with all processes activated, and 40 km with the scattering/friction combination. In the Barents sea, and in particular in the eastern part of Svalbard, MIZ exceeds 150 km with all processes, and 300 km with scattering and viscous friction activated . In Figure 12, all processes have been combined. At 3:00 a.m. on May 2, 2010, large floes are present at the ship position ($c > 0.8$ and $D_{\max} \simeq 200m$) associated with small waves ($H_s < 1$ m). Broken ice is nevertheless not far from the ship position and break-up occurs earlier than reported in Collins et al. (2015), so that at 6:00 p.m the ship is surrounded by small floes and encounters waves with $Hs \simeq 1.5\ m$. Wave height, which is over 4 m in open water, rapidly decreases into the ice cover due to the turbulence effects. Reducing the roughness length or the creep parameter B can affect the results significantly, in particular the breaking extent and H_s values at the location of R/V Lance.

5. Discussion

The observed non-linear behavior of wave attenuation when ice is broken is generally consistent with the expected effects of creep, and Arctic-wide simulations of ice attenuation and break-up appear reasonable when combining under-ice friction and creep. A more convincing validation would nevertheless requires a variety of cases with accurate observations of the ice properties (floe size, thickness and concentration...) evolution during a wave event. Besides, the creep parameter B is very sensitive to the thickness and temperature of the ice (e.g. Cole et al., 1998), and here we have used a constant temperature of 270 K. Taking the value at the freezing point could lead to overestimate its induced attenuation, likewise, the use of the mean ice thickness certainly leads to an underestimation of the wave dissipation. Besides, creep is expected to occur in large floes or unbroken ice areas, and therefore does not explain wave attenuation reported in the first kilometers of the MIZ (Wadhams et al., 1986). Latter cases could be explained by scattering, friction, floe-floe collisions, slamming (Bennetts et al., 2015), and overflow (Toffoli et al., 2015), but their respective magnitude is left to be quantified in real conditions. Although our scattering model is strongly simplified, with isotropic energy redistribution, it is generally consistent with Wadhams et al. (1986) observations of the spectrum widening within the ice covered sea. Such an increase in directional spread has not been observed in SAR imagery of waves with periods longer than 8 s (Ardhuin et al., 2017). This is consistent with the limited effect of scattering found when using the approach of Bennetts and Squire (2012). Scattering could very well dominates for shorter wave periods within the first kilometers of the sea ice cover. Some other dissipation mechanism, like friction below the ice, is an indispensable companion to creep, without which the wave amplitude would keep unrealistically large values (5 cm or more) where the amplitude is too low to produce a significant creep dissipation. Unfortunately, the roughness length for the wave motion is a sensitive but poorly known parameter. From our study, it appears that choosing a value 1 *cm* leads to consequent attenuation in the case of large wave heights, independently from the size of the floes. It disagrees with Kohout et al. (2014) and Collins et al. (2015), where high waves are reported far into the ice cover.

Finally, the counter-intuitive effects observed with the creep dissipation were partly due to the choice of using the waves in the ice dispersion relation, considerably increasing the wavelengths of high-frequency waves. This increase can extent so that waves become more than 3 times larger than the floes. In these conditions, the assumption of a semi-infinite elastic plate on which relies the dispersion relation looses its validity. The same applies for scattering coefficient, also computed following a semi-infinite ice cover, especially for long period waves. In the perspective of improving waves-in-ice modelling towards realism, it could therefore be an interest to investigate the effects of the floe size on the wave propagation.

6. Conclusion

The effect of sea ice on ocean waves, including the influence of floe sizes, has been implemented in the spectral wave model WAVEWATCH III, following the previous developments of Dumont et al. (2011) and Williams et al. (2013a) with monochromatic waves. These include the update of the floe size at each wave model time step depending on the ocean wave properties. Because scattering and creep are strongly dependent on floe sizes, the ice break up introduces a feedback on the wave field with interesting evolution patterns. First scattering leads to an increase in wave height and directional spread as documented by Wadhams et al. (1986). This increase in wave height can lead to a more break-up of the ice cover and a stronger attenuation in the presence of dissipation, due to an increase in the average effective propagation time across a given region (see the diffuse arrivals in figure 3 of Ardhuin et al., 2016). On the contrary, creep produces a dissipation that is strongest for high waves and unbroken ice, during the cyclic flexure of the ice. When the ice is broken, we assumed that creep dissipation was only significant for floes larger than 0.3 times the wavelength. This transition from a strong dissipation to no dissipation is able to reproduce the qualitative behavior reported in Collins et al. (2015), with a strong wave attenuation in unbroken ice and a weak attenuation ice the ice is broken. Our simulations suggest that scattering and creep are not enough and that another dissipation process is necessary to provide a strong enough background dissipation. Indeed, scattering only redistributes it in all directions, and creep vanishes when the ice is broken into small floes or when the wave height gets very small. A plausible mechanism is under-ice friction, as implemented here following Stopa et al. (2016b), with an ice roughness of the order of 1 cm. A further investigation of these effects will probably require the coupling to an ice model that can advect the floe size distribution and properly reproduce the increase of the maximum floe size when floes are frozen together.

Appendix A. Creep dissipation for random waves

Using the flow law for ice given by Glen (1955), Wadhams (1973) expressed the energy dissipation rate per unit surface in a thin elastic plate of sea ice as the integral of the volumetric dissipation across the plate,

$$\frac{dE_t}{dt} = \int_0^{h_i} |\sigma_{xx}^4/(2B)^3| dx. \tag{A.1}$$

We note that in Wadhams (1973), the ice thickness is $2h_i$. From this expression, Wadhams (1973) derived that in the case of a monochromatic wave (with height $H_i = 2a_i$ in the ice), the evolution of the wave height

$$\frac{d < (H_i/2)^2 > /2}{dx} = -\frac{K h_i^5 I_3}{32\lambda_i^8 C_g R\rho g} < (H_i/2)^4 > \tag{A.2}$$

with

$$\begin{aligned} K &= \tfrac{[Y^* k^2/(1-\nu^2)]^4}{5(2B)^3} & \text{(A.3)} \\ I_3 &= \tfrac{1}{\pi}\int_0^\pi \sin^4\beta d\beta = 3/8. & \text{(A.4)} \end{aligned}$$

Assuming a random sea state with a Rayleigh distribution, we can linearize the dissipation rate,

$$\frac{dE_t}{dt} = -\alpha_{creep} E_{ice}. \tag{A.5}$$

We note that for the Rayleigh distribution we have

$$< (H_i/2)^4 > = 2\left(\frac{H_{rms,i}}{2}\right)^4 = 2(2E_{ice})^2, \tag{A.6}$$

which gives

$$\alpha_{creep} = \frac{8}{32 \times 5} C_g \frac{K h_i^5 I_3}{\lambda_i^4 C_g R\rho g} \times \frac{E_{ice} k^4}{(2\pi)^4} \tag{A.7}$$

Replacing $E_{ice} k^4/(2\pi)^4$ by the curvature of dominant waves, we finally get

$$\alpha_{creep} = \frac{3}{160}\left(\frac{Y^*}{2B(1-\nu^2)}\right)^4 \frac{h_i^5}{\lambda_i^4 R\rho g} \times \left(\frac{Cg}{RC_{g,i}}\right)\int_{0.7k_i}^{1.3k_i} k_i^4 E(k) dk \tag{A.8}$$

Finally, in β_{creep}, we multiply α_{creep} by F given by eq. (17), which is a heuristic smooth transition from unbroken to broken ice, so that the dissipation gradually goes to 0 for waves much longer than the floe sizes, because in that case the ice does not deform and so does not dissipate wave energy.

Acknowledgments. G.B. and F.A. are supported by DGA, ANR grants ANR-14-CE01-0012 MIMOSA, ANR-10-LABX-19-01, EU-FP7 project SWARP under grant agreement 607476, ONR grant number N0001416WX01117. This work has been carried out as part of the Copernicus Marine Environment Monitoring Service (CMEMS) ArcticMix project. CMEMS is implemented by Mercator Ocean in the framework of a delegation agreement with the European Union.

References

Ardhuin, F., Chapron, B., Collard, F., Smith, M., Stopa, J., Thomson, J., Doble, M., Wadhams, P., Blomquist, B., Persson, O., Collins, III, C. O., 2017. Measuring ocean waves in sea ice using sar imagery: A quasi-deterministic approach evaluated with sentinel-1 and in situ data. Remote Sensing of Environment 189, 211–222.

Ardhuin, F., Rogers, E., Babanin, A., Filipot, J.-F., Magne, R., Roland, A., van der Westhuysen, A., Queffeulou, P., Lefevre, J.-M., Aouf, L., Collard, F., 2010. Semi-empirical dissipation source functions for wind-wave models: part I, definition, calibration and validation. J. Phys. Oceanogr. 40 (9), 1917–1941.

Ardhuin, F., Sutherland, P., Doble, M., Wadhams, P., 2016. Ocean waves across the Arctic: attenuation due to dissipation dominates over scattering for periods longer than 19 s. Geophys. Res. Lett. 43.

Asplin, M. G., Galley, R., Barber, D. G., Prinsenberg, S., 2012. Fracture of summer perennial sea ice by ocean swell as a result of arctic storms. J. Geophys. Res. 117, C06025.

Banner, M. L., Babanin, A. V., Young, I. R., 2000. Breaking probability for dominant waves on the sea surface. J. Phys. Oceanogr. 30, 3145–3160. URL http://ams.allenpress.com/archive/1520-0485/30/12/pdf/i1520-0485-30-12-3145.pdf

Bennetts, L. G., Alberello, A., Meylan, M. H., Cavaliere, C., Babanin, A. V., Toffoli, A., Dec. 2015. An idealised experimental model of ocean surface wave transmission by an ice floe. Ocean Modelling 96, 85–92.

Bennetts, L. G., Squire, V. A., 2012. On the calculation of an attenuation coefficient for transects of ice-covered ocean. Proc. Roy. Soc. Lond. A 468, 132–162.

Cole, D. M., Johnson, R. A., Durell, G. D., 1998. Cyclic loading and creep response of aligned first-year sea ice. J. Geophys. Res. 103 (C10), 21,751–21,758.

Collins, III, C. O., Rogers, W. E., Marchenko, A., Babanin, A. V., 2015. In situ measurements of an energetic wave event in the Arctic marginal ice zone. Geophys. Res. Lett. 42, 1863–1870.

de Carolis, G., Olla, P., Pignagnoli, L., 2005. Effective viscosity of grease ice in linearized gravity waves. Journal of Fluid Mechanics 535, 369–381.

de Laplace, P. S., 1776. Suite des recherches sur plusieurs points du système du monde (XXV–XXVII). Mém. Présentés Acad. R. Sci. Inst. France , 542–552.

Dee, D. P., Uppala, S. M., Simmons, A. J., Berrisford, P., Poli, P., Kobayashi, S., Andrae, U., Balmaseda, M. A., Balsamo, G., Bauer, P., Bechtold, P., Beljaars, A. C. M., van de Berg, L., Bidlot, J., Bormann, N., Delsol, C., Dragani, R., Fuentes, M., Geer, A. J., Haimbergere, L., Healy, S. B., Hersbach, H., Holm, E. V., Isaksena, L., øallberg, P. K., Köhler, M., Matricardi, M., McNally, A. P., Monge-Sanz, B. M., Morcrette, J.-J., Park, B.-K., Peubey, C., de Rosnay, P., Tavolato, C., Thépaut, J.-N., Vitart, F., 2011. The era-interim reanalysis: configuration and performance of the data assimilation system. Quart. Journ. Roy. Meteorol. Soc. 137, 553–597.

Dumont, D., Kohout, A., Bertino, L., 2011. A wave-based model for the marginal ice zone including a floe breaking parameterization. J. Geophys. Res. 116, C00E03.

Filipot, J.-F., Ardhuin, F., 2012. A unified spectral parameterization for wave breaking: from the deep ocean to the surf zone. J. Geophys. Res. 117, C00J08.

Glen, J. W., 1955. The creep of polycrystalline ice. In: Proceedings of the Royal Society of London A: Mathematical, Physical and Engineering Sciences. Vol. 228. The Royal Society, pp. 519–538.

Grant, W. D., Madsen, O. S., 1979. Combined wave and current interaction with a rough bottom. J. Geophys. Res. 84, 1797–1808.

Kohout, A. L., 2008. Water wave scattering by floating elastic plates with application to sea-ice. Ph.D. thesis, ResearchSpace@ Auckland.

Kohout, A. L., Meylan, M. H., 2008. An elastic plate model for wave attenuation and ice floe breaking in the marginal ice zone. J. Geophys. Res. 113, C09016.

Kohout, A. L., Williams, M. J. M., Dean, S. M., Meylan, M. H., 2014. Storm-induced sea-ice breakup and the implications for ice extent. Nature 509, 604–607.

Liu, A. K., Holt, B., Vachon, P. W., 1991. Wave propagation in the marginal ice zone' model predictions and comparisons with buoy and synthetic aperture radar data. J. Geophys. Res. 96 (C3), 4605–4621.

Liu, A. K., Mollo-Christensen, E., 1988. Wave propagation in a solid ice pack. J. Phys. Oceanogr. 18, 1702–1712.

Masson, D., LeBlond, P. H., 1989. Spectral evolution of wind-generated surface gravity waves in a dispersive ice field. J. Fluid Mech. 202 (7), 43–81.

Mellor, M., 1986. Mechanical Behavior of Sea Ice. In: Untersteiner, N. (Ed.), The Geophysics of Sea Ice. NATO ASI Series. Springer US, pp. 165–281.

Meylan, M., Squire, V. A., 1996. Response of a circular ice floe to ocean waves. J. Geophys. Res. 101 (C4), 8869–8884.

Meylan, M. H., Masson, D., 2006. A linear boltzmann equation to model wave scattering in the marginal ice zone. Ocean Modelling 11, 417–427.

Montiel, F., Squire, V. A., Bennetts, L. G., 2016. Attenuation and directional spreading of ocean wave spectra in the marginal ice zone. J. Fluid Mech. 790, 492–522.

Mosig, J. E. M., Montiel, F., Squire, V. A., 2015. Comparison of viscoelastic-type models for ocean wave attenuation in ice-covered seas. J. Geophys. Res. 120, 6072–6090.

Nghiem, S. V., Rigor, I. G., Clemente-Colón, P., Neumann, G., Li, P. P., 2016. Geophysical constraints on the antarctic sea ice cover. Remote sensing of Environment 181, 281–292.

Nye, J. F., 1953. The flow law of ice from measurements in glacier tunnels, laboratory experiments and the jungfraufirn borehole experiment. In: Proceedings of the Royal Society of London A: Mathematical, Physical and Engineering Sciences. Vol. 219. The Royal Society, pp. 477–489.

Rogers, W. E., Thomson, J., Shen, H. H., Doble, M. J., Wadhams, P., Cheng, S., 2016. Dissipation of wind waves by pancake and frazil ice in the autumn beaufort sea. J. Geophys. Res. 121.

Sakov, P., Counillon, F., Bertino, L., Lisæter, K. A., Oke, P. R., Korablev, A., 2012. Topaz4: an ocean-sea ice data assimilation system for the north atlantic and arctic. Ocean Science 8 (4), 633–656.
URL http://www.ocean-sci.net/8/633/2012/

Squire, V., Aug. 2007. Of ocean waves and sea-ice revisited. Cold Regions Science and Technology 49 (2), 110–133.

Squire, V., Dugan, J., Wadhams, P., Rottier, P., Liu, A., 1995. Of ocean waves and sea ice. Annu. Rev. Fluid Mech. 27 (3), 115–168.

Stopa, J. E., Ardhuin, F., Bababin, A., Zieger, S., 2016a. Comparison and validation of physical wave parameterizations in spectral wave models. Ocean Modelling 103, 2–17.

Stopa, J. E., Ardhuin, F., Girard-Ardhuin, F., 2016b. Wave climate in the arctic 1992-2014: seasonality and trends. The Cryosphere 10, 1605–1629.

Stopa, J. E., Ardhuin, F., Husson, R., Jiang, H., Chapron, B., Collard, F., 2016c. Swell dissipation from 10 years of envisat asar in wave mode. Geophys. Res. Lett. 43, 3423–3430.

Stroeve, J., Holland, M. M., Meier, W., Scambos, T., Serreze, M., 2007. Arctic sea ice decline: Faster than forecast. Geophys. Res. Lett. 34, L09501.

Strong, C., 2012. Atmospheric influence on Arctic marginal ice zone position and width in the Atlantic sector, FebruaryApril 19792010. Climate Dynamics 39 (12), 3091–3102.

The WAVEWATCH III ® Development Group, 2016. User manual and system documentation of WAVEWATCH III ® version 5.16. Tech. Note 329, NOAA/NWS/NCEP/MMAB, College Park, MD, USA, 326 pp. + Appendices.

Thomson, J., Rogers, W. E., 2014. Swell and sea in the emerging Arctic Ocean. Geophys. Res. Lett. 41, 3136–3140.

Toffoli, A., Bennetts, L. G., Meylan, M. H., Cavaliere, C., Alberello, A., Elsnab, J., , Monty, J. P., 2015. Sea ice floes dissipate the energy of steep ocean waves. Geophys. Res. Lett. 42, 8547–8554.

Tolman, H. L., 2003. Treatment of unresolved islands and ice in wind wave models. Ocean Modelling 5, 219–231.

Tolman, H. L., Booij, N., 1998. Modeling wind waves using wavenumber-direction spectra and a variable wavenumber grid. Global Atmos. Ocean Syst. 6, 295–309.

Wadhams, P., 1973. Attenuation of swell by sea ice. J. Geophys. Res. 78 (18), 3552–3563.

Wadhams, P., Squire, V. A., Ewing, J. A., Pascal, R. W., 1986. The effect of the marginal ice zone on the directional wave spectrum of the ocean. J. Phys. Oceanogr. 16, 358–376.

Wang, R., Shen, H. H., Jun. 2010. Gravity waves propagating into an ice-covered ocean: A viscoelastic model. Journal of Geophysical Research: Oceans 115 (C6), C06024.

Williams, T. D., Bennetts, L. G., Squire, V. A., Dumont, D., Bertino, L., 2013a. Wave-ice interactions in the marginal ice zone. part 1: Theoretical foundations. Ocean Modelling 70, 81–91.

Williams, T. D., Bennetts, L. G., Squire, V. A., Dumont, D., Bertino, L., 2013b. Wave-ice interactions in the marginal ice zone. part 2: Numerical implementation and sensitivity studies along 1d transects of the ocean surface. Ocean Modelling 71, 92–101.

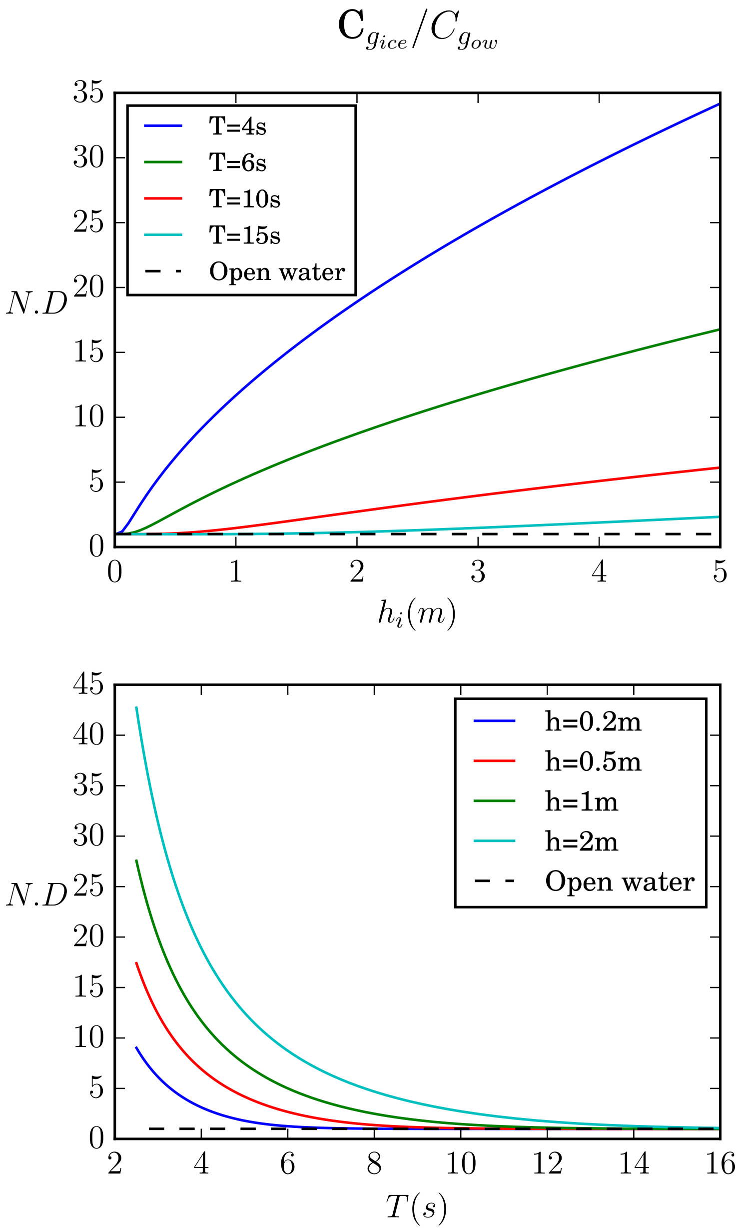

Figure 1: Top: evolution of $C_{g,i}/C_g$ according to the ice thickness in the case of deep water, i.e. $k_i D \gg 1$, for 4 different wave periods. Bottom: same parameter for 4 values of the ice thickness h_i. The black dashed line represents the asymptote of the open water group velocity.

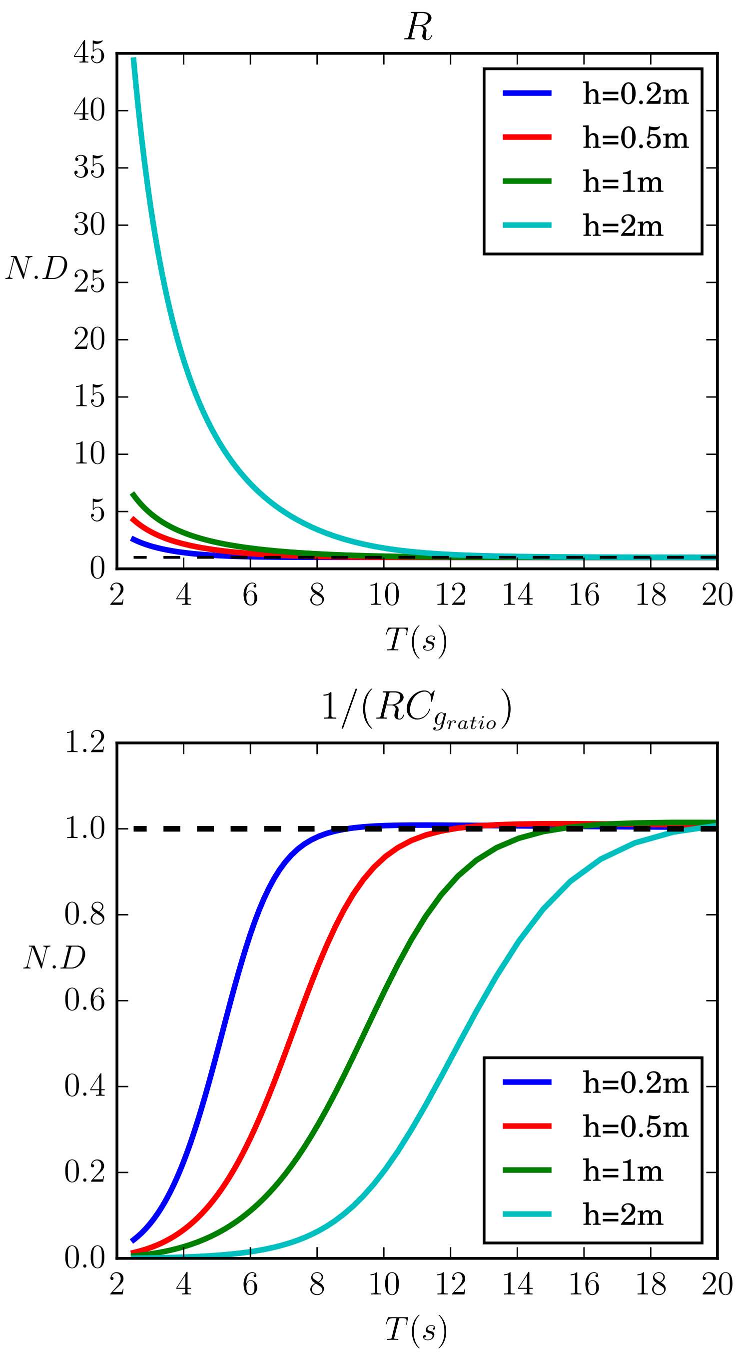

Figure 2: Top: R as defined by Wadhams (1973), as a function of the wave period, in the case of deep water and for 4 values of the thickness h_i, 20 cm, 50 cm, 1 m and 2 m. Bottom: change in elevation variance given by the energy flux conservation $a_i^2/a^2 = C_g/RC_{g,i}$.

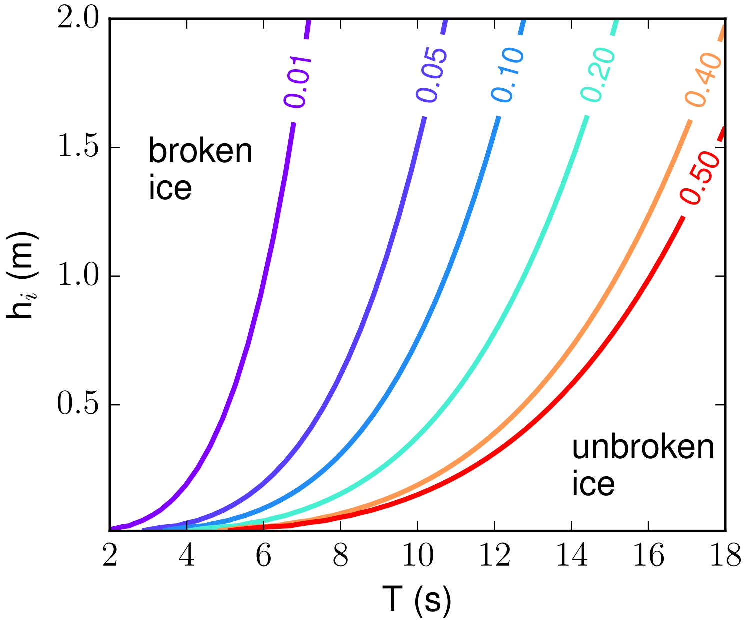

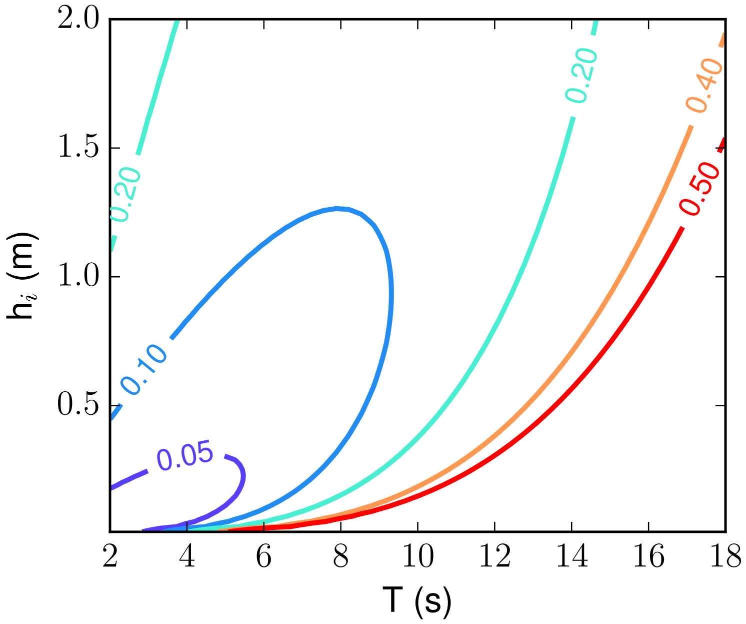

Figure 3: Minimum significant wave height (H_s) triggering flexural failure with Williams et al. (2013a) parametrization (top) and ours (bottom) as a function of wave period T (s) and ice thickness h_i (m), supposing a narrow wave spectrum.

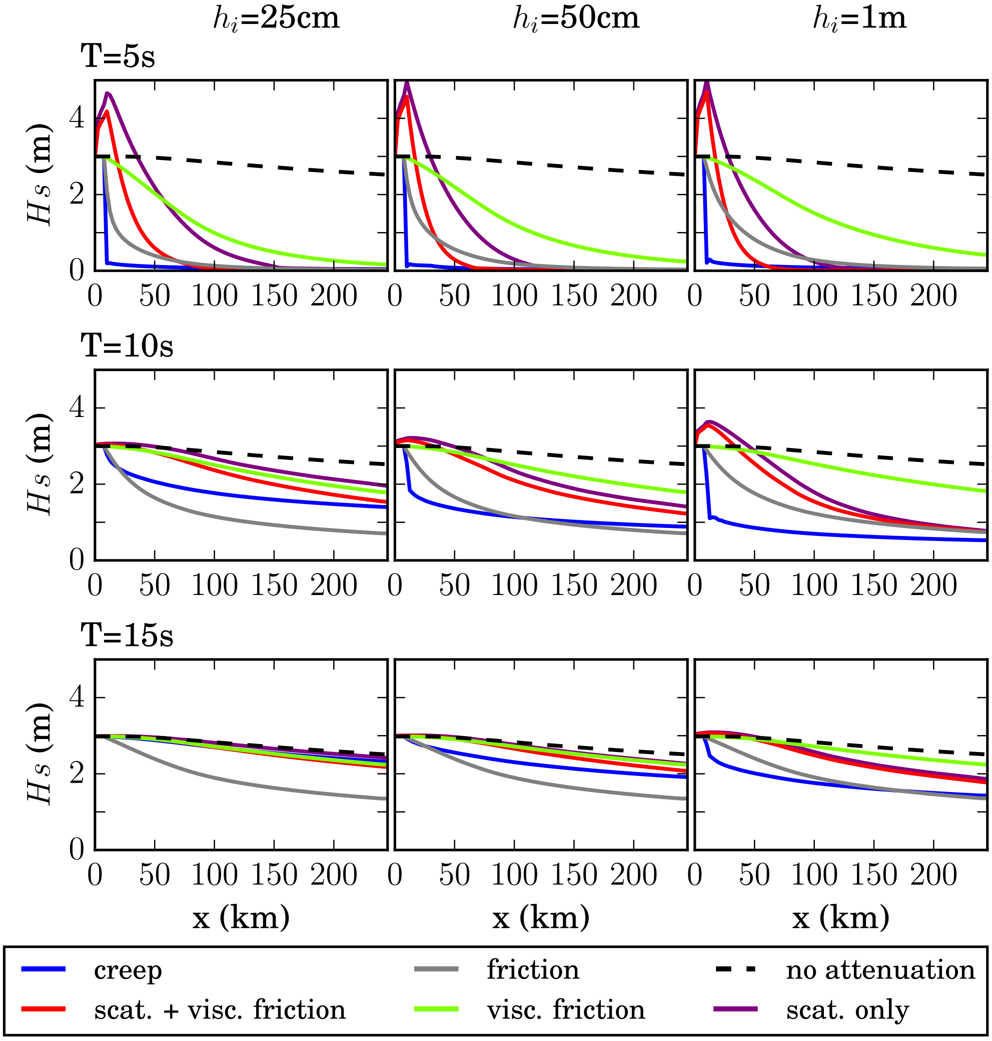

Figure 4: Distribution of H_s along the x-direction at the center of the domain, for different peak periods (T_p = 5, 10, 15 s) and ice thickness (h_i = 0.25, 0.5, 1 m). Different colors correspond to the activation of different processes.

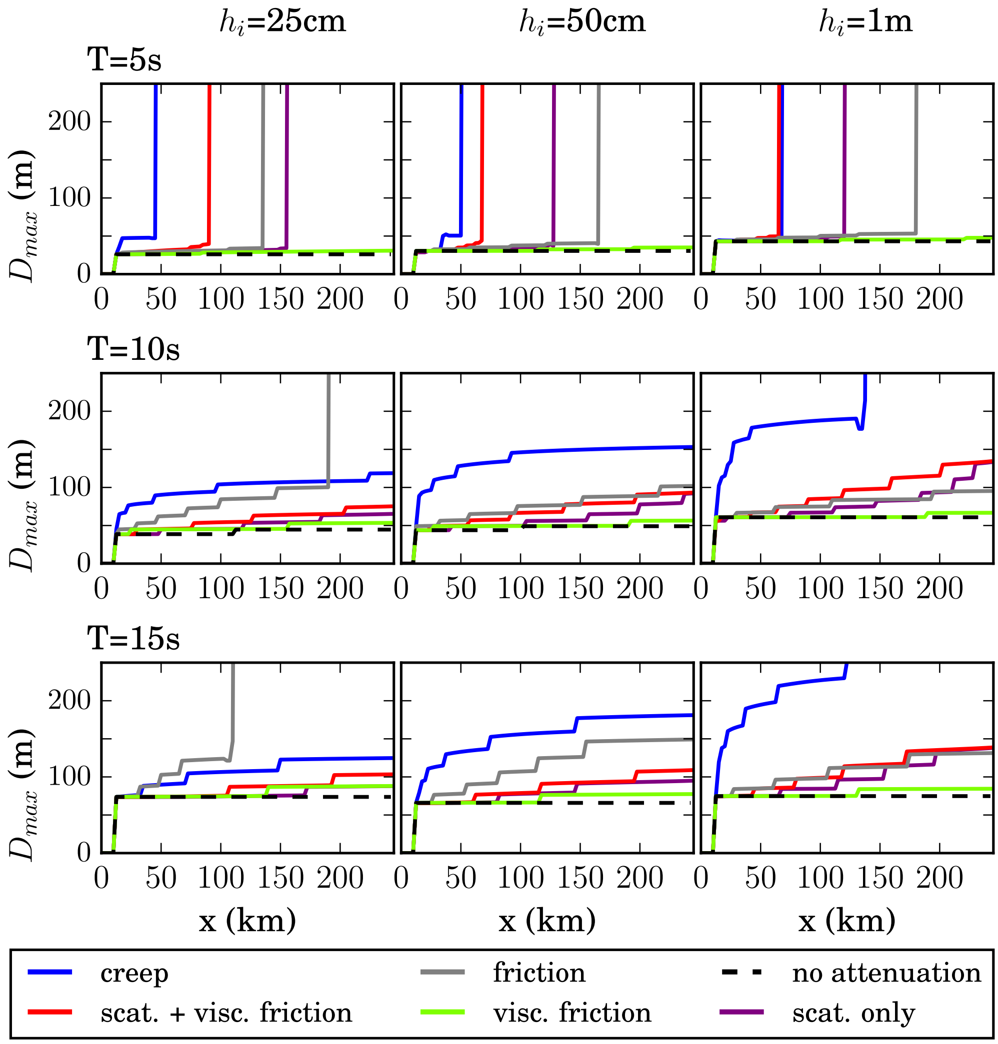

Figure 5: Distribution of $D_{\max}$ along the x-direction at the center of the domain, for different peak periods ($T_p = 5$, 10, 15 s) and ice thickness ($h_i = 0.25$, 0.5, 1 m). Different colors correspond to the activation of different processes.

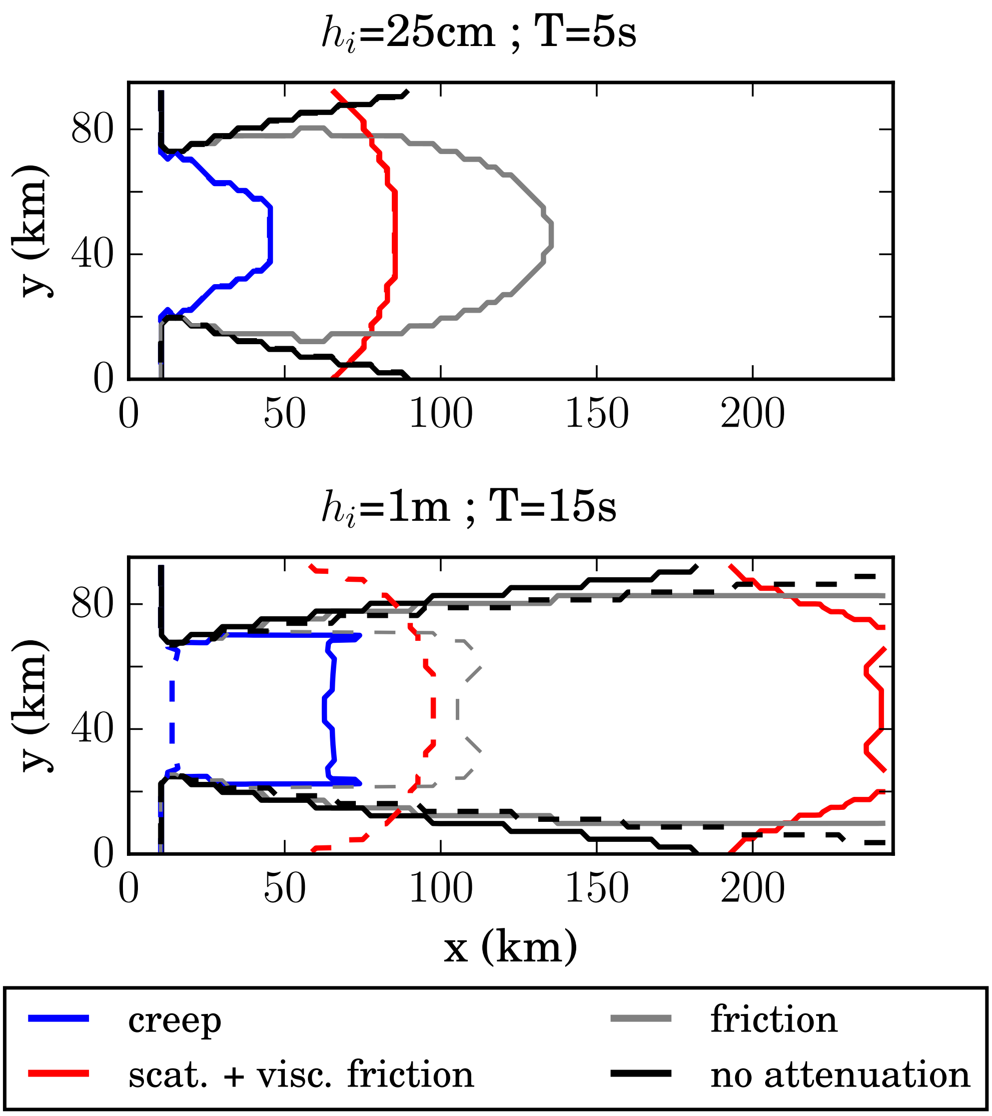

Figure 6: Distribution of $D_{\max}$ for different peak periods and ice thickness . In each panel, solid lines represent the contour $D_{\max} = 200$ m, and dashed lines the contour $D_{\max} = 100$ m, showing the extent of broken ice.

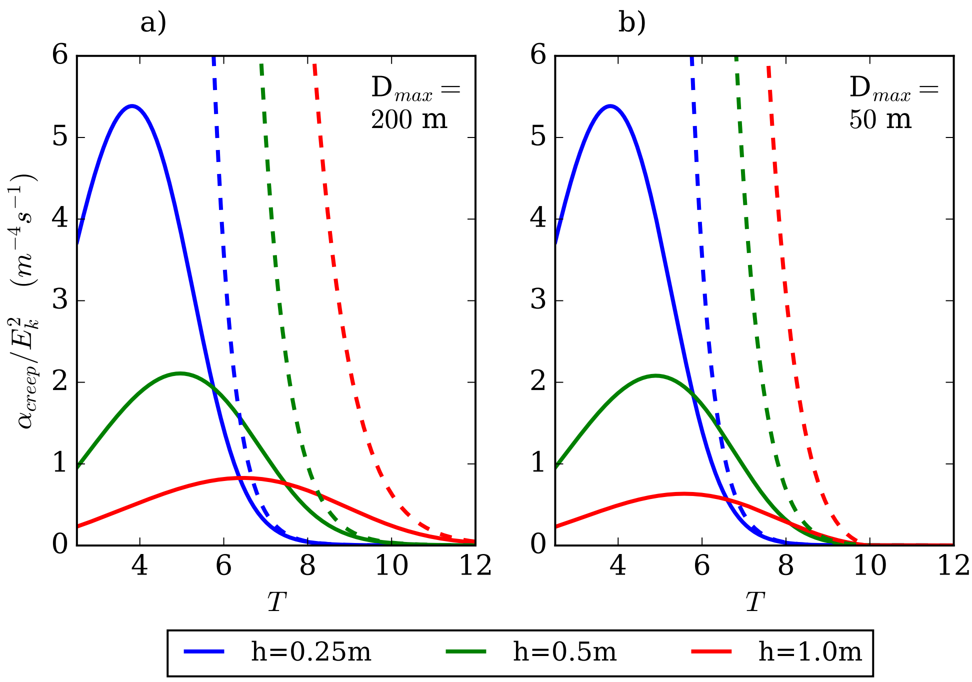

Figure 7: Creep attenuation (α_{creep})for different $D_{\max}$. The attenuation rate has been divided by E_k^2 to show its evolution independently from the wave amplitude. Solid lines represent (α_{creep}/E_k^2) evolution with the wave period T (s) and dashed lines represent the same thing without the effect of $C_g/RC_{g,i}$.).

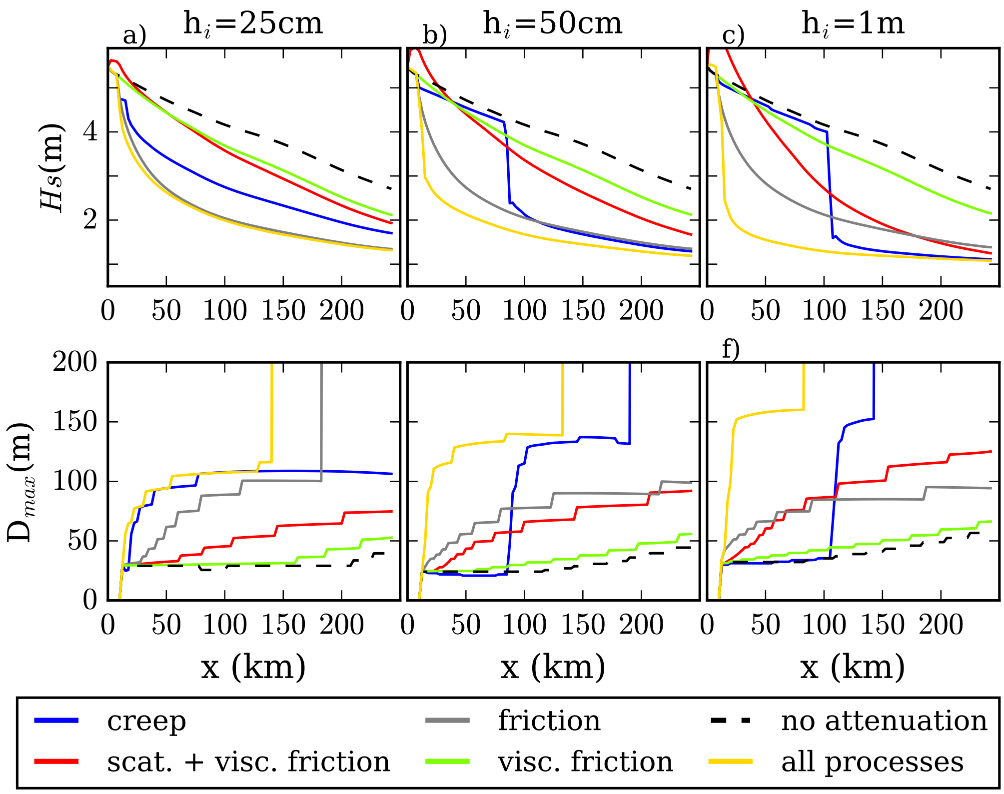

Figure 8: Distribution of H_s (up) and $D_{\max}$ (down) along the x-direction at the center of domain, for different ice thickness ($h_i = 0.25,\ 0.5,\ 1\ m$). Different colors correspond to the activation of different processes.

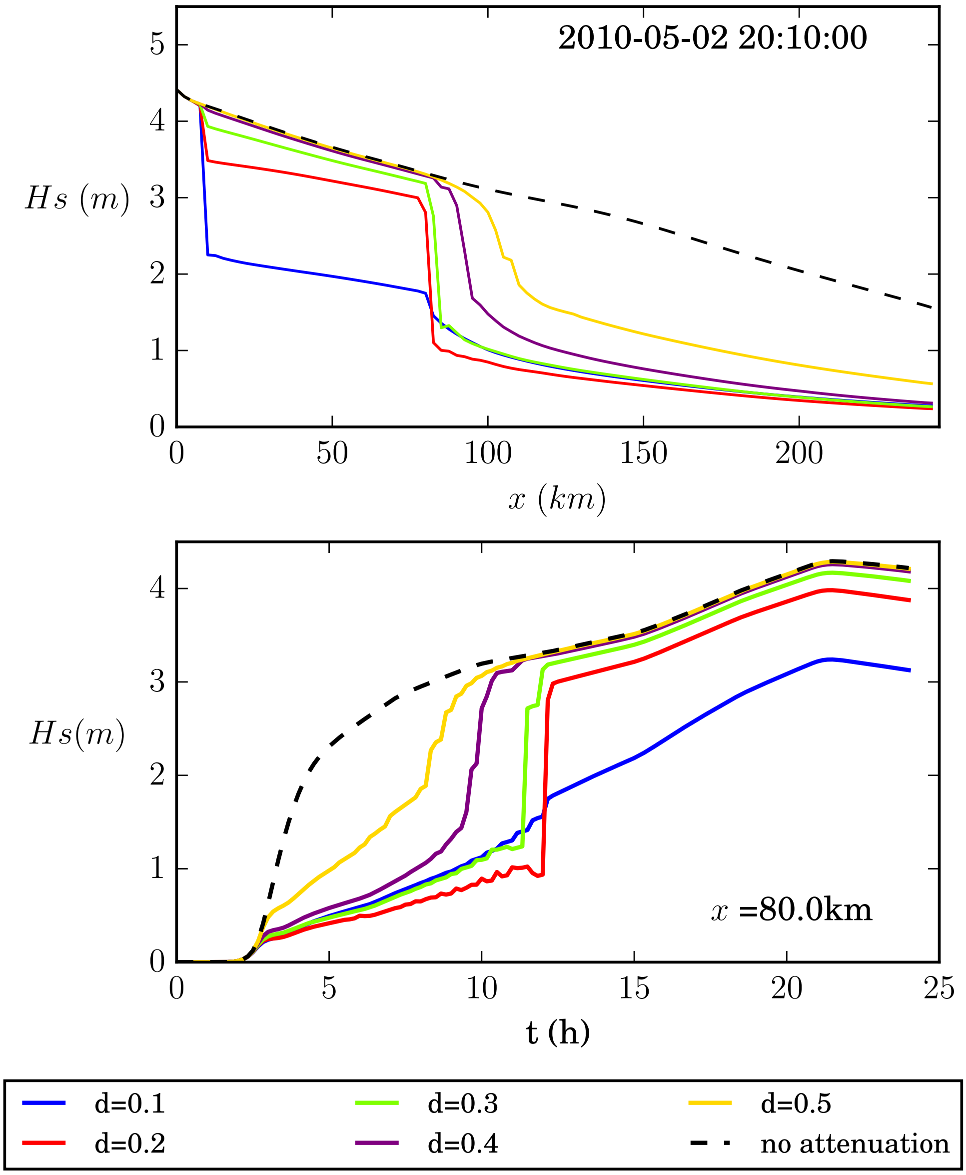

Figure 9: Evolution of H_s spatially (up) and temporally (down), at the center of the domain for the academic test reproducing the Svalbard observation of May 2, 2010. The run starts at 8:00 a.m. on May2, 2010. Each color represents a different tuning of C_λ. **??**

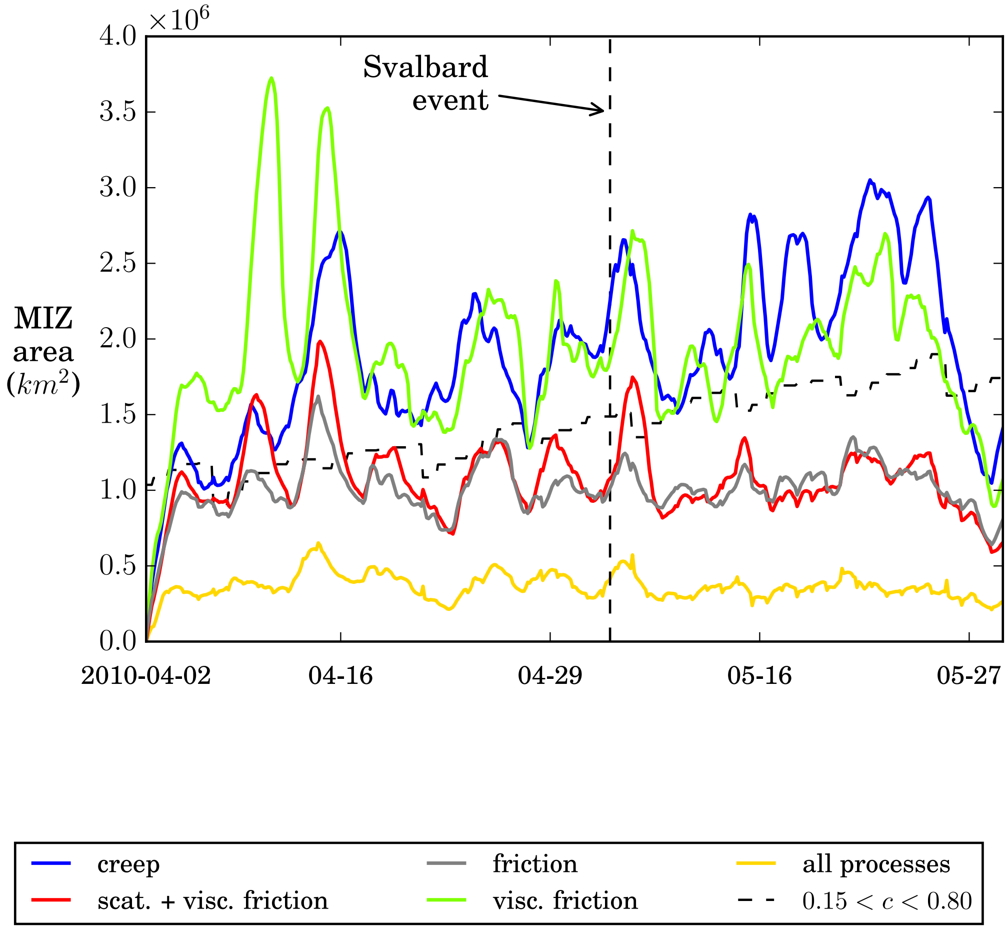

Figure 10: The MIZ area as computed in April-May 2010. The MIZ is defined as the region for which $c > 0$ and $D_{\max} < 1000\ m$. The dashed black line represents the MIZ area according to the criterion given by : $c < 0.9$

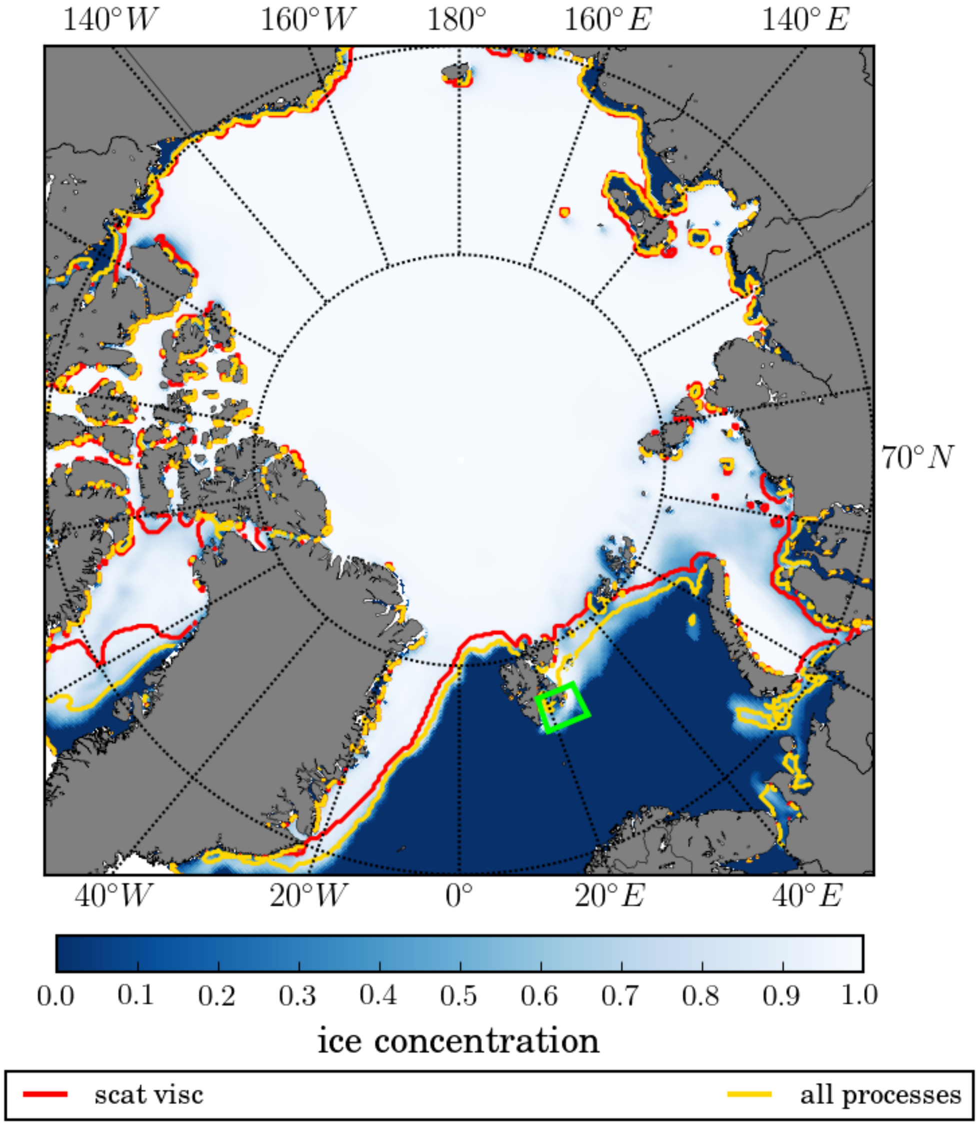

Figure 11: $D_{\max} < 1000m$ contour for two different combinations of processes on May 3rd, 2010, at 00:00. The green square delimits the area represented in Figure 12.

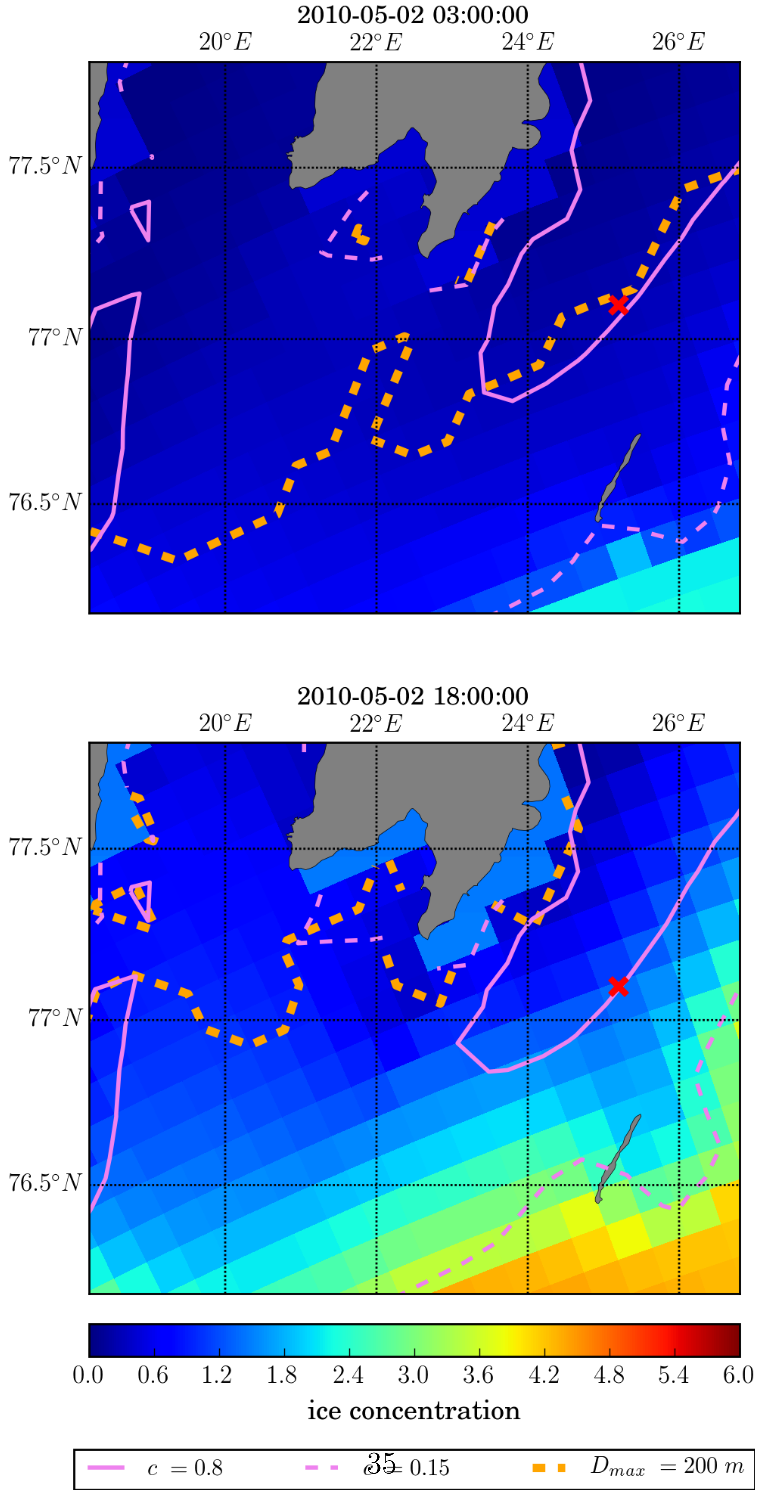

Figure 12: $D_{\max}$ = 100 m, and ice concentration c = 0.8 and c = 0.15 contours are plotted over H_s distribution in Svalbard on May 2, 2010, before (up) and during the storm (down). The red cross represents the location of the R/V Lance from which the observation reported by Collins et al. (2015) have been gathered. For this run, the 3 attenuation processes were combined.

)